

# **Inorganic Acid-derived Hydrogen-bonded Organic Frameworks to Form Nitrogen Rich Carbon Nitride for Photocatalytic Hydrogen Evolution**

Yunqi Tang,<sup>a</sup> Meng Yuan,<sup>a</sup> Baojiang Jiang,<sup>\*a</sup> Yuting Xiao,<sup>a</sup> Yu Fu,<sup>b</sup> Shuai Chen,<sup>c</sup>  
Zhaopeng Deng,<sup>a</sup> Qingjiang Pan,<sup>a</sup> Chungui Tian,<sup>a</sup> Honggang Fu<sup>\*a</sup>

<sup>a</sup> Key Laboratory of Functional Inorganic Material Chemistry, Ministry of Education of P. R. China, Heilongjiang University, Harbin, P. R. China;

\*E-mail: fuhg@vip.sina.com, fuhg@hlju.edu.cn; jiangbaojiang88@sina.com

<sup>b</sup> Jilin University;

<sup>c</sup> Analytical Instrumentation Center, Institute of Coal Chemistry, Chinese Academy of Sciences, Taiyuan, P. R. China.

## Contents

**Figure S1.** N<sub>2</sub> adsorption/desorption isotherm and pore size distribution (insert) of pristine CN, MS-1, MN-1 and MCl-1 calculated by using NLDFT model.

**Table S1.** BET Area of CN, MS-1, MN-1 and MCl-1.

**Figure S2.** The TGA-MS spectrum of MNP-1.

**Figure S3.** The TGA-MS spectrum of MCIP-1.

**Figure S4.** The comparison of XRD patterns between MSP-1 and previous work in database.

**Figure S5.** The comparison of XRD patterns between MNP-1 and previous work in database.

**Figure S6.** The comparison of XRD patterns between MCIP-1 and previous work in database.

**Figure S7.** The molecular arrangement of MSP-1 in the unit cell with the influence of hydrogen bonding interactions.

**Figure S8.** The molecular arrangement of MNP-1 in the unit cell with the influence of hydrogen bonding interactions.

**Figure S9.** The molecular arrangement of MCIP-1 showing the hydrogenbond-like interactions.

**Figure S10.** XRD patterns with adjusting concentrations of sulfuric acid to as-prepared carbon nitride under the same condition with MS-1.

**Table S2.** The diverse structural shapes of N content (N wt%) of CN, MS-1, MN-1 and MCl-1

**Figure S11.** FT-IR spectra of the as-prepared samples CN (a), MS-1(b), MN-1(c) and MCl-1(d).

**Figure S12.** H<sub>2</sub> production rate for CN, MS-1, MN-1, and MCl-1 samples under the irradiation of 300 W Xe lamp with 450nm bandpass filter.

**Table S3.** Comparison of photocatalytic water splitting based on C<sub>3</sub>N<sub>4</sub> matters.

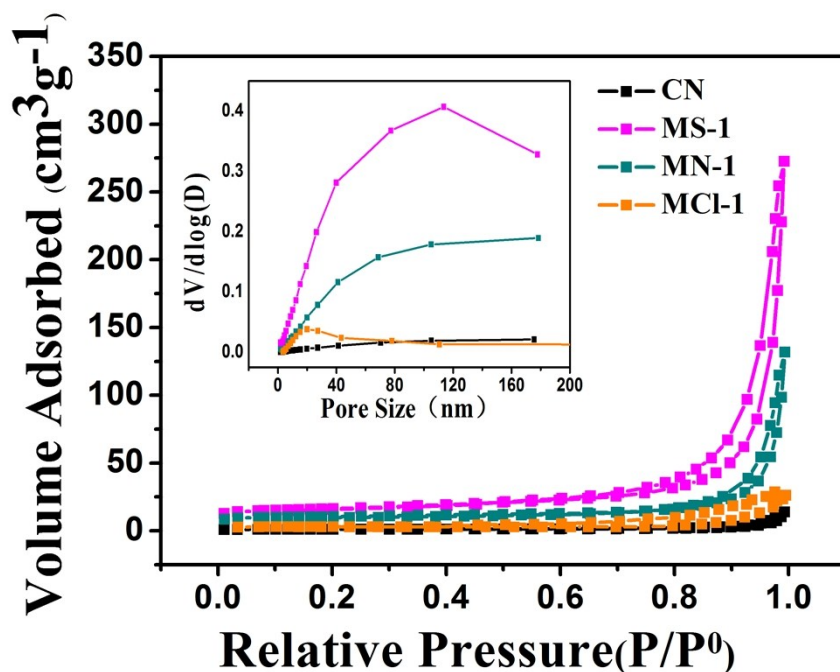


**Figure S1.** (a)  $N_2$  adsorption/desorption isotherm and (b) pore size distribution of CN, MS-1, MN-1 and MCI-1 calculated by using NLDFT model.

**Table S1.** BET Area of CN, MS-1, MN-1 and MCI-1

Name	CN	MS-1	MN-1	MCI-1
BET Area ( $m^2g^{-1}$ )	3.78	68.02	35.81	10.19

The **Figure S1.** (a) and **Table S1.** show the BET isotherm and specific surface area of CN, MS-1, MN-1 and MCI-1, respectively. It also indicates the presence of pore structure formed by layer structure, and the BET areas of four samples are in order of MS-1 ( $68.02 m^2g^{-1}$ ) > MN-1 ( $35.81 m^2g^{-1}$ ) > MCI-1 ( $10.19 m^2g^{-1}$ ) > CN ( $3.78 m^2g^{-1}$ ).

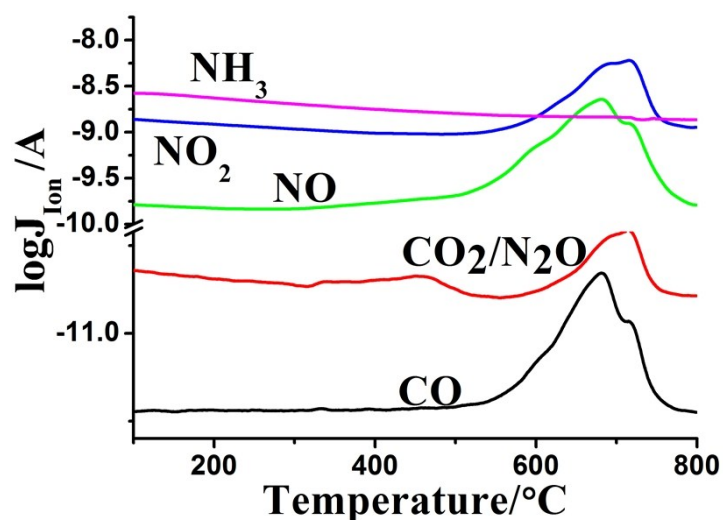


**Figure S2.** The TGA-MS spectrum of MNP-1. Indicates varying decomposition product of MNP-1 throughout heating process. All the resultants ( $\text{NO}_2$ ,  $\text{NO}$ ,  $\text{CO}_2/\text{N}_2\text{O}$  and  $\text{CO}$ ) are start to be detected around  $500^\circ\text{C}$ , which corresponds to the weight loss at  $350^\circ\text{C}$  in TGA curves. The D-value of temperature can be attributed to the rapid heating rate and the mistiming of resultants reach to mass spectrum detector.

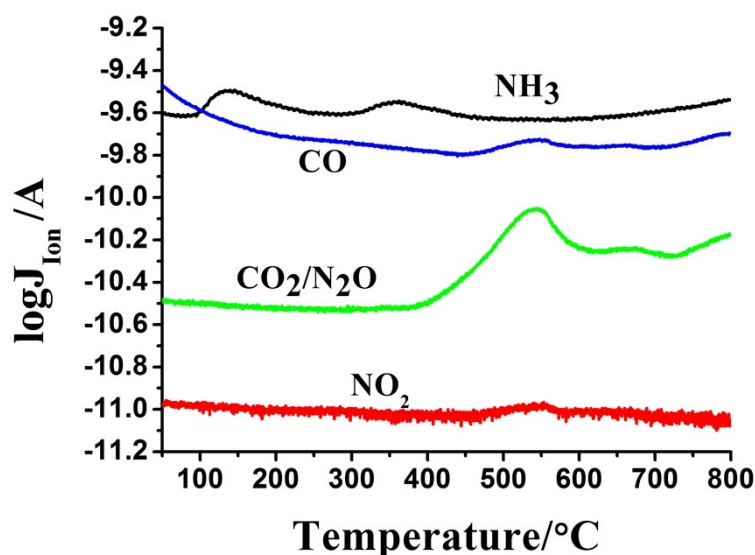


**Figure S3.** The TGA-MS spectrum of MCIP-1. It shows thermogravimetric-related mass spectrum of MCIP-1 throughout heating process. The  $\text{NH}_3$  have two peaks at  $150^\circ\text{C}$  and  $350^\circ\text{C}$ , corresponding to dissociation of  $-\text{NH}_3$  group and decomposition of melamine, respectively. The generation of  $\text{CO}$ ,  $\text{CO}_2$  and  $\text{N}_2\text{O}$  at  $550^\circ\text{C}$  represents the formation of carbon nitride.

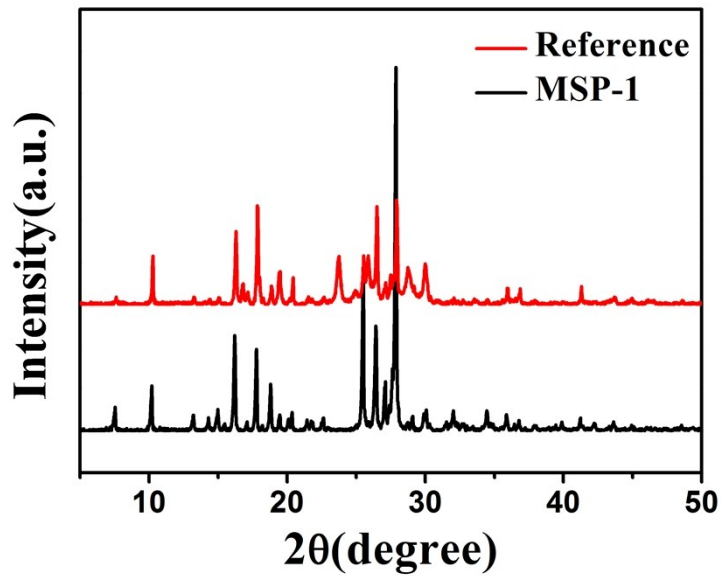


**Figure S4.** The comparison of XRD patterns between MSP-1 and previous work in database.

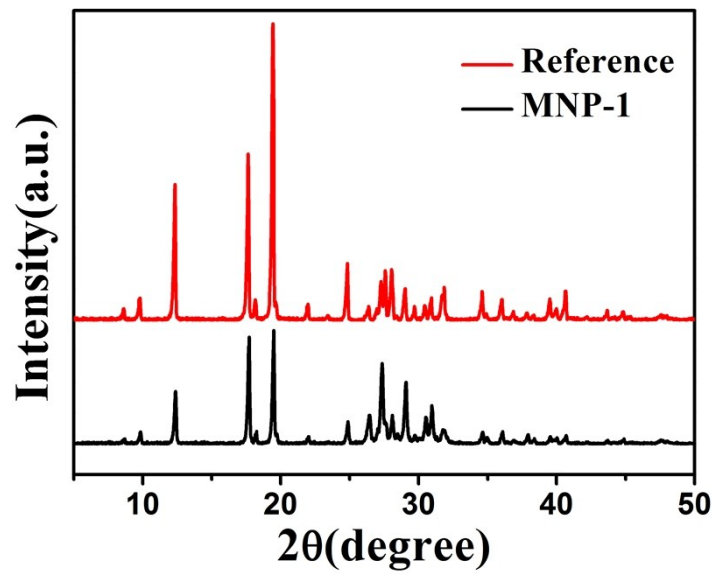


**Figure S5.** The comparison of XRD patterns between MNP-1 and previous work in database.

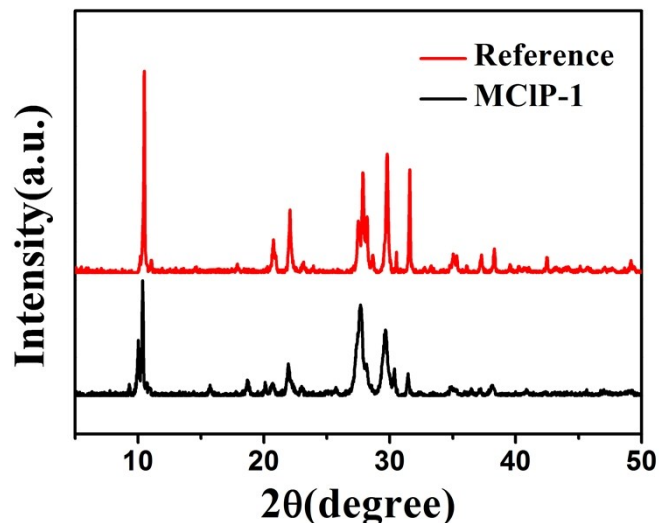


**Figure S6.** The comparison of XRD patterns between MCIP-1 and previous work in database. **Figure S4-S6.** show that the main peak in XRD patterns among MSP-1, MNP-1 and HLMCIP-1 are identical to corresponding reference patterns in database, respectively. The result indicates that the obtained MSP-1, MNP-1 and MCIP-1 are all HOF-like structure which are similar to certified references.

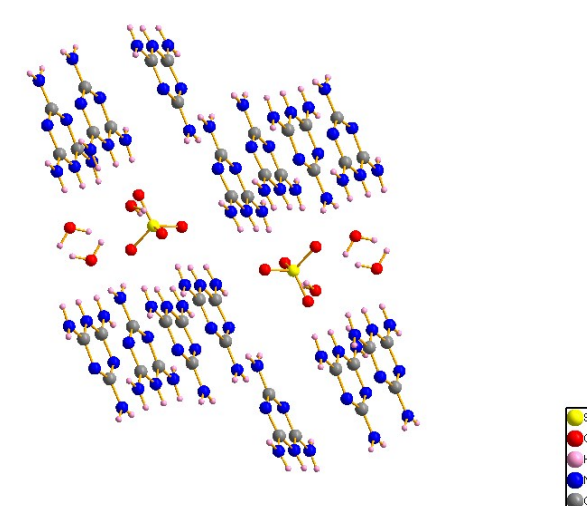


**Figure S7.** The molecular arrangement of MSP-1 in the unit cell with the influence of hydrogen bonding interactions. The water molecules form a hydrogen-bonded dimeric structure, and the sulfate connected with a water molecule as well. Subsequently, the above molecules are combined with six melamine to form a layer by hydrogen bonds, and different layers are bonded by two melamine molecules via  $\pi$ - $\pi$  stacking together with in-layer melamine molecules.

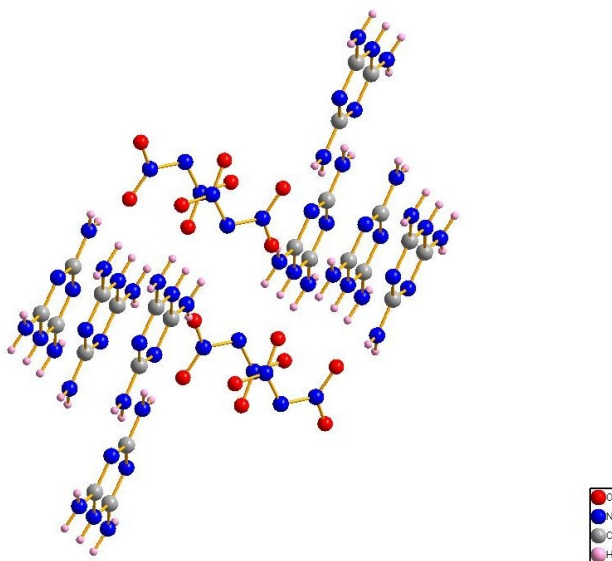


**Figure S8.** The molecular arrangement of MNP-1 in the unit cell with the influence of hydrogenbonding interactions. Firstly, the crystal contains one monoprotonated melaminium cation and one dinitramide anion by ionization. After that, the oxygen in dinitramide play a role as acceptor to combine with other three melamine molecules, and HOF-like melaminium dinitramide is obtained eventually.

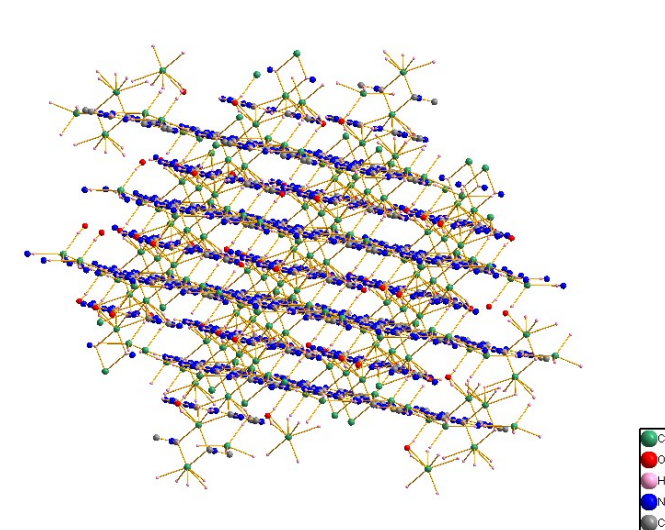


**Figure S9.** The molecular arrangement of MCIP-1 showing the hydrogen bonding-like interactions. We can see that efficient packing of the ions is obtained through a complex network with a formation similar to hydrogen bonding interaction.

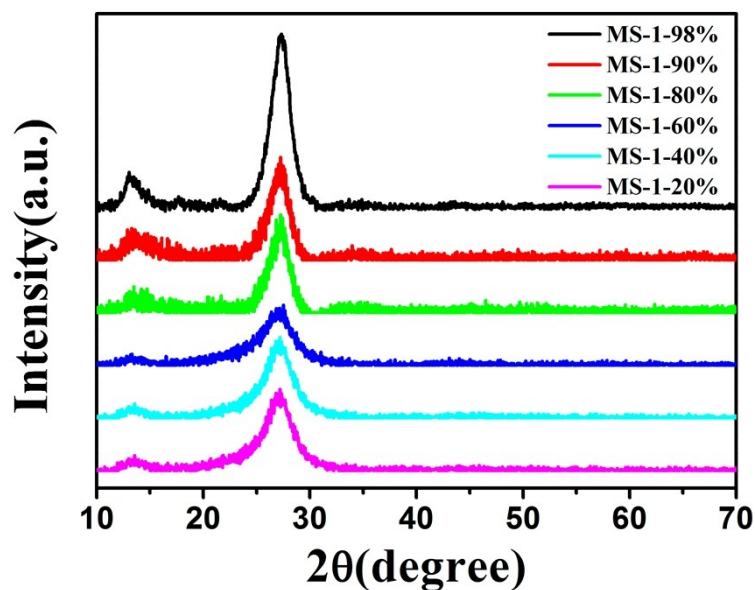


**Figure S10.** XRD patterns with adjusting concentrations of sulfuric acid to as-prepared carbon nitride under the same condition with MS-1. The intensity of characteristic peak at  $13.0^\circ$  grows up with the amount of water content decrease, which indicates the ratio of in-plane packing is decreased with the loss of water content.

**Table S2.** The diverse structural shapes of N content (N wt %) of CN, MS-1, N-1 and MCI-1.

Sample N	C-N=C (N wt %)	N-C3 (N wt %)	C-NH (N wt %)
CN	41.54	5.09	4.24
MS-1	39.49	12.60	2.72
MN-1	37.86	10.09	3.15
MCI-1	32.87	8.43	5.77

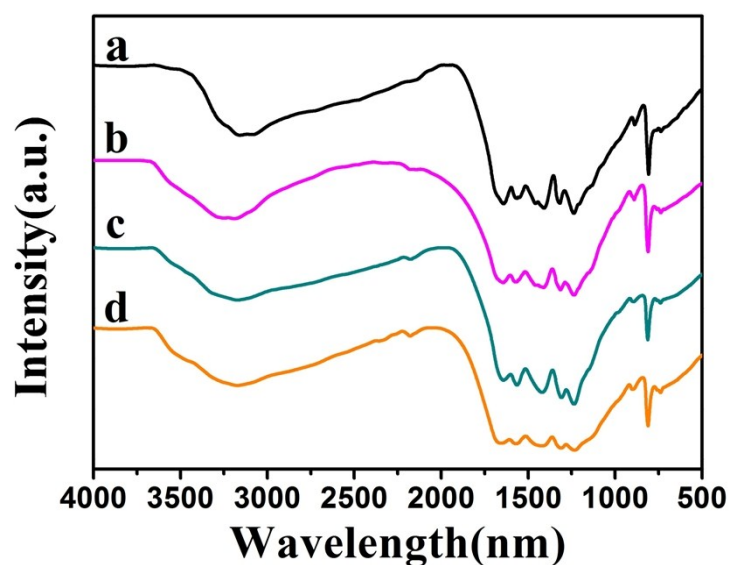


**Figure S11.** FT-IR spectra of the as-prepared samples CN (a), MS-1(b), MN-1(c) and MCl-1(d).

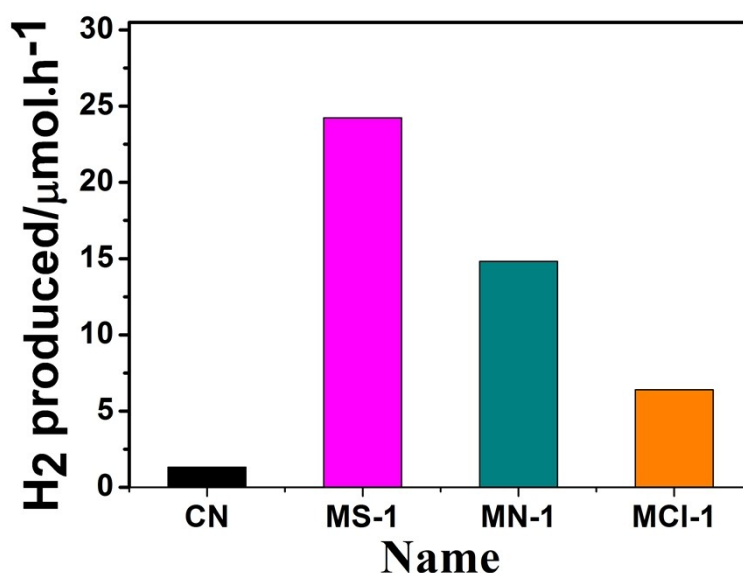


**Figure S12.** Photocatalytic H<sub>2</sub> production rate for CN, MS-1, MN-1, and MCl-1 samples under the irradiation of 300 W Xe lamp with 450nm bandpass filter.

Because the light filter with longer wavelength provides lower energy to the system, all the samples show relative lower photocatalytic hydrogen production. Under this condition, the three as-prepared samples show better photocatalytic activity than CN; further prove the high content of N is conducive to great performance. And MS-1 still exhibits the highest photocatalytic hydrogen efficiency, due to the additional S doping, at 24.23μmol per hour.

**Table S3.** Comparison of photocatalytic water splitting based on C<sub>3</sub>N<sub>4</sub> matters.

Sacrificial Electron Donor	Cocatalyst	Weight of sample (g)	Hydrogen Evolution Rate ( $\mu\text{mol h}^{-1}$ )	Transformational amount ( $\mu\text{mol g}^{-1} \text{h}^{-1}$ )	Reference
10 vol %	1 wt%	0.05	75.03	\	Ref.1
15 vol%	3 wt%	0.01	1.8	\	Ref.2
10 vol%	0	0.05	8.1	\	Ref.3
10 wt%	3 wt%	0.05	71.5	1430.1	Ref.4
10 vol%	3 wt%	0.10	49.3	\	Ref.5
10 vol%	3 wt%	0.10	45.5	454.94	Ref.6
10 vol%	3 wt%	0.05	53	\	Ref.7
20 vol%	1 wt%	0.05	79.8	1596	Ref.8
20 vol%	3 wt%	0.03	81.01	\	This work

#### Reference

1. P. M. Ramos, J. M. Gil, R.C. Dante, F. Vaquer, R.M. Navarro, J. L.G. Fierro, *International Journal of Hydrogen Energy*, 2015, **40**, 7273-7281.
2. Q. Gu, Y. S. Liao, L. S. Yin, J. L. Long, X. X. Wang, C. Xue, *Applied Catalysis B: Environmental*, 2015, **165**, 503-510.
3. Y. Chen, B. Lin, H. Wang, Y. Yang, H. B. Zhu, W. L. Yu, J. M. Basset, *Chemical Engineering Journal*, 2016, **286**, 339-346.
4. L.Q. Yang, J. F. Huang, L. Shi, L. Y. Cao, Q. Yu, Y. N. Jie, J. Fei, H. B. Ouyang, J. H. Ye, *Applied Catalysis B: Environmental*, 2017, **204**, 335-345.
5. X. M. Bu, Y. Bu, S. W. Yang, F. Sun, L. F. Tian, Z. Peng, P. He, J. Sun, T. Huang, X. Y. Wang, G. Q. Ding, J. H. Yang and X. M. Xie, *RSC Adv.*, 2016, **6**, 112210-112214.
6. Y. F. Yang, J. J. Chen, Z. Y. Mao, N. An, D. J. Wang and B. D. Fahlman, *RSC Adv.*, 2017, **7**, 2333-2341.
7. J. R. Ran, T. Y. Ma, G. P. Gao, X. W. Du and S. Z. Qiao, *Energy Environ. Sci.*, 2015, **8**, 3708-3717.
8. H. H. Ou, L. H. Lin, Y. Zheng, P. J. Yang, Y. X. Fang, and X. C. Wang, *Adv. Mater.*, 2017, **29**, 1700008.